Available online at www.sciencedirect.com
SCIENCE DIRECT®
Computational Materials Science xxx (2006) xxx–xxx
COMPUTATIONAL MATERIALS SCIENCE
www.elsevier.com/locate/commatsci

Portevin–LeChatelier effect in Al–Mg alloys: Influence of obstacles – experiments and modelling

H. Dierke [a,*], F. Krawehl [a], S. Graff [b], S. Forest [b], J. Šachl [a], H. Neuhäuser [a]

[a] Institut für Physik der Kondensierten Materie, TU Braunschweig, Mendelssohnstr. 3, 38106 Braunschweig, Germany
[b] Centre des Matériaux/UMR 7633, Ecole des Mines de Paris/CNRS, BP 87, 91003 Evry, France

Received 12 October 2005; received in revised form 9 February 2006; accepted 9 March 2006

Abstract

Due to their low weight and high mechanical strength Al–Mg alloys provide a large variety of applications as material for lightweight construction. However, the practical benefit is limited due to instabilities and inhomogeneities caused by correlated movement of dislocations during plastic deformation (Portevin–LeChatelier effect, PLC). By addition of unshearable obstacles the formation of dislocation avalanches should be prevented or at least reduced. Uniaxial tension tests at various constant strain rates on the metal matrix composite (MMC) AA5754 with 2 or 5 vol.% Al_2O_3 particles showed hardly any influence of the particles added. This could be explained by an inhomogeneous distribution of the particles during manufacturing of this MMC. First results of FE simulations using a macroscopic PLC model are presented. The importance of local stress concentrations around the inclusions is emphasized.

Keywords: Al–Mg alloys; Portevin–LeChatelier effect; Plastic instabilities; Metal matrix composites

1. Introduction

Some of the earliest and most prominent examples for materials with PLC plastic instabilities are Al-based alloys, e.g. [1–6], where the effect occurs around room temperature in an appropriate range of deformation rates. The instabilities, which show up as repeated load drops (serrations) during continuous deformation, are associated with local plastic shear in slip bands and sometimes propagating deformation bands. They cause corrugations of the originally smooth specimen surface and may give rise to early failure of the components. In view of the high importance of Al alloys for light-weight constructions, attempts have been made to suppress the PLC effect or to shift its range of occurrence to non-critical values. The latter is possible as the understanding of the mechanisms that control the PLC effect is rather advanced today, e.g. [7–18] and successful modelling has been achieved, e.g. [19–24].

The PLC instabilities arise if the waiting times t_w of dislocations at obstacles are in the order of the diffusion times t_d of solutes towards or along dislocations (''dynamic strain ageing'', DSA) and if intensive interaction of dislocations [13–15] through their long-range stress field results in an avalanche initiated by the dislocation segments escaped from their Cottrell solute cloud and multiplying rapidly. Thus the PLC effect does not occur either if $t_w \gg t_d$, so that the dislocations are always saturated with solutes, or if $t_w \ll t_d$, so that a diffusionial rearrangement of the obstacles cannot occur during the short waiting time. The waiting time t_w can be adapted by choosing the deformation rate $\dot{\varepsilon}(\sim 1/t_w)$.

Another attempt to suppress PLC behaviour is to avoid the development of dislocation avalanches by introducing appropriate obstacles. It is well-known from earlier studies (e.g. [1–6]) that the PLC effect in Al–Mg(–Si) alloys is best pronounced in as-quenched alloys, while ageing mostly reduces the PLC serrations due to the production of small precipitates acting as dislocation obstacles. First systematic studies of this approach have been started by Pink [25–27]

* Corresponding author.
E-mail address: h.dierke@tu-braunschweig.de (H. Dierke).

0927-0256/$ - see front matter © 2006 Elsevier B.V. All rights reserved.
doi:10.1016/j.commatsci.2006.03.019

and the Prague group [28–30], and has been discussed in some detail by Brechet and Estrin [31] who indicated the complexity of the problem. For instance, if the obstacles are not strong enough and can be cut (and thereby diminished) by the dislocations, they may have the opposite effect and enhance the development of large dislocation groups by the obstacle destruction mechanism (cf. [32,33]). Recent results about PLC effects in alloys with precipitates have been reported in [34–40].

In this work we explore the possibility of suppressing the PLC effect by the addition of unsurmountable obstacles in an Al–Mg alloy, namely small alumina particles. They are expected to be sufficiently strong not to be cut by dislocations, so no obstacle destruction and development of large dislocation groups should occur. In the following we show some first experimental (Section 3) as well as some modeling (Section 4) results in comparison, and draw conclusions for future improvement of this approach.

2. Experimental

Uniaxial tensile tests have been performed at room temperature and at constant applied strain rates varying from $10^{-6}\,s^{-1}$ to $10^{-3}\,s^{-1}$. For the experiments flat specimens with a size of 54 mm × 4 mm × 1.5 mm have been used, prepared from polycrystalline cold–rolled sheets of Al–3%Mg alloy (AA5754), reinforced by Al_2O_3 particles with an average diameter of about 3 μm (matrix and reinforced material produced by LKR Ranshofen, Austria). All specimens are heat treated in air for recovery after rolling (5 h at 673 K) and quenched in water.

The investigated samples are the parent Al–3%Mg alloy as well as the materials containing particles, noted as the AA5754 metal–matrix composite (MMC). Two volume fractions of particles are considered (2 vol.% and 5 vol.%). Unfortunately, during manufacturing of the MMCs, the Al_2O_3 particles tend to form clusters, separated by rather large areas of pure matrix material. This inhomogeneous distribution of particles reduces significantly the benefit of the introduction of non-shearable obstacles for dislocation movement.

Examples of stress–strain curves for various strain rates from $1\times10^{-6}\,s^{-1}$ to $1\times10^{-3}\,s^{-1}$ are shown in Fig. 1. From these curves three quantities have been evaluated: (a) the yield stress σ_y (at the transition from elastic to plastic flow), (b) the critical strain ε_c for the onset of the PLC serrations and (c) $\Delta\sigma$, the magnitude of the PLC stress drops, characterizing the strength of the PLC effect.

3. Experimental results and their discussion

3.1. Yield stress

The change of the plastic behaviour with ageing has been studied for the matrix first and then for the MMCs. As a first characteristic quantity the yield stress σ_y is plotted in Fig. 2 versus ageing treatment. The yield stress increases slightly with ageing from the "as quenched" up to the most strongly annealed condition (combination of 120 h at room temperature followed by 120 h at 140 °C). The corresponding microstructures as observed by TEM are shown in Fig. 3, indicating a gradual rather sluggish growth of precipitates in this AA5754 alloy. Surprisingly, the yield stress of MMCs is neither higher than that of the matrix as expected, nor does it notably change with annealing treatment or alumina content. This contradicts the simple "classical" strengthening concept according to which the strong inclusions should result in an increased yield stress. We interpret this observation as an indication for high local stress concentrations in the surroundings of the inclusions. These stress concentrations may already arise from specimen preparation (heat treatments) due to the different thermal expansion coefficients of matrix and particles. They may increase further during loading in the

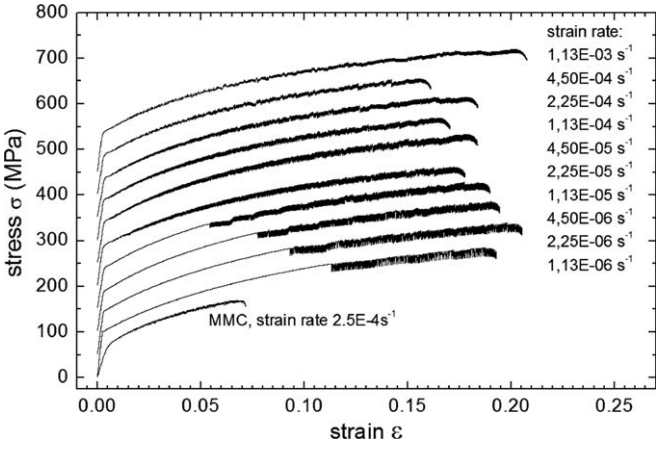

Fig. 1. Macroscopic stress–strain curves for various strain rates from $1\times10^{-6}\,s^{-1}$ to $1\times10^{-2}\,s^{-1}$ (AA5754 matrix). For better view the curves are vertically displaced by 50 MPa. For comparison also the stress–strain curve of one MMC measurement is shown (bottom curve).

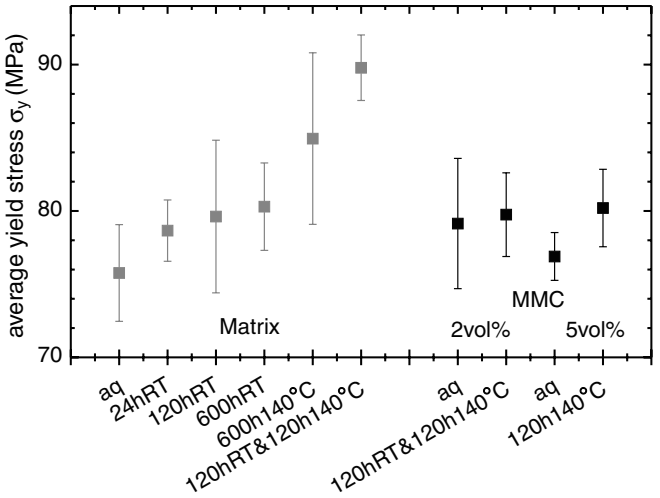

Fig. 2. Average yield stress σ_y for the different ageing treatments and materials.

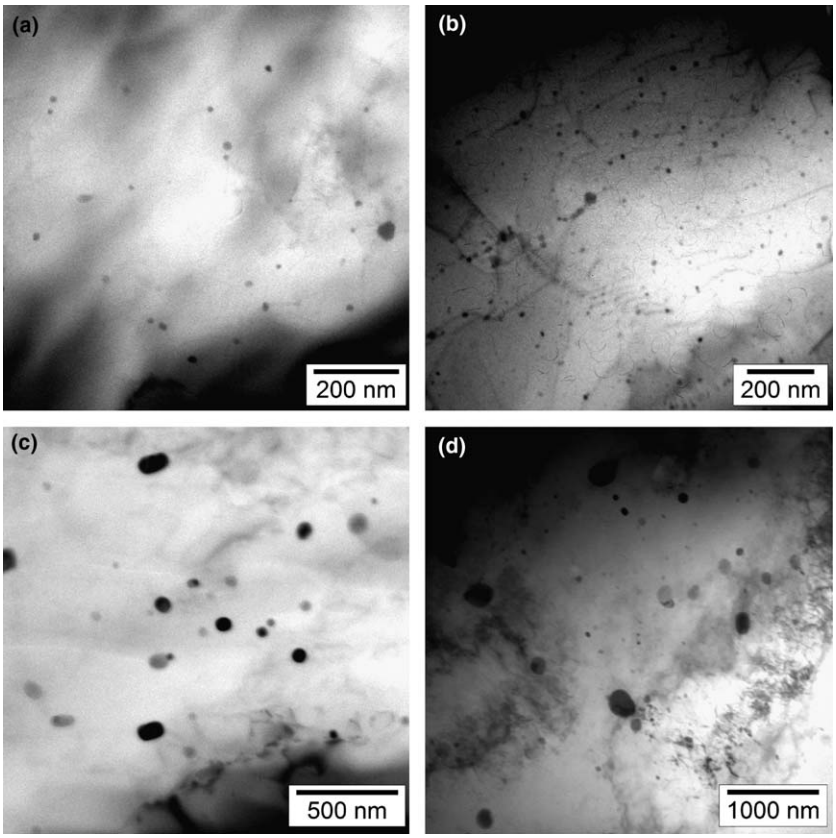

Fig. 3. TEM images of the microstructure: (a) as quenched, (b) after 600 h at room temperature, (c) after 600 h at 140 °C and (d) after 120 h at room temperature followed by 120 h at 140 °C.

elastic range due to different elastic moduli and result in early local plasticity around the inclusions at a reduced average applied stress. This causes a more extended micro-yield region of the MMC compared to the matrix alloy as seen in Fig. 1. With longer annealing and development of precipitates, their strengthening effect of the matrix seems to be compensated by increasing stress concentrations (cf. Section 4).

3.2. Critical strain for PLC onset

As can be seen in Fig. 1, the PLC effect sets in for low strain rates only after a certain smooth strain ε_c which shows a pronounced dependence on strain rate (Fig. 4(a) and (b)). In agreement with the results in [5,16,17,42], the PLC starts already at the yield point for strain rates $\dot{\varepsilon} > 5 \times 10^{-4}\ s^{-1}$, while with lower strain rates an increasing pre-strain is required for the onset of PLC serrations. This behaviour, which reflects the necessity of a certain dislocation population for the expression of the PLC effect, is called "inverse" PLC effect, because it contradicts on first sight the waiting time argument in Section 1. However, as shown in [11–14,41] such behaviour is well compatible with DSA, if the evolution of the additional DSA enthalpy [15,16,18] and of the dislocation density is properly considered. According to [16,18] the inverse behaviour, which is associated with type C serrations (nucleation, no propagation) at very low strain rates, occurs with saturated DSA enthalpy, while normal behaviour, associated with type A (continuous propagation) at high strain rates is due to the exhaustion of DSA, i.e. reduced DSA enthalpy, so PLC can operate right after the yield point.

The annealing treatments of this AA5754 alloy do not clearly show the expected suppression of PLC (Fig. 4(a)), and no effect of the slight strengthening by precipitates can be detected in the large scatter of critical strain values.

For the MMCs the expected suppression of PLC instabilities also cannot be observed in our specimens (Fig. 4(b)) at least for the low strain rates, rather the onset on PLC seems to start even slightly earlier than for the pure matrix as also found in [42]. Again this is supposed to be the consequence of stress concentrations at the inclusions, where first plastic activity starts with the development of dislocation avalanches already at rather low external stresses. In addition, as the distribution of the Al_2O_3 particles in our specimens is very inhomogeneous (as well in size as in space, showing pronounced clustering), there seems to be always space enough between those clusters to develop large dislocation avalanches, similar as in the matrix. It should also be noted that in some specimens micro-cracks could be observed even by the optical microscope starting from alumina inclusions, sometimes causing early failure of the specimen. Such local damage has been observed and investigated in similar MMCs in [43]. A very slight

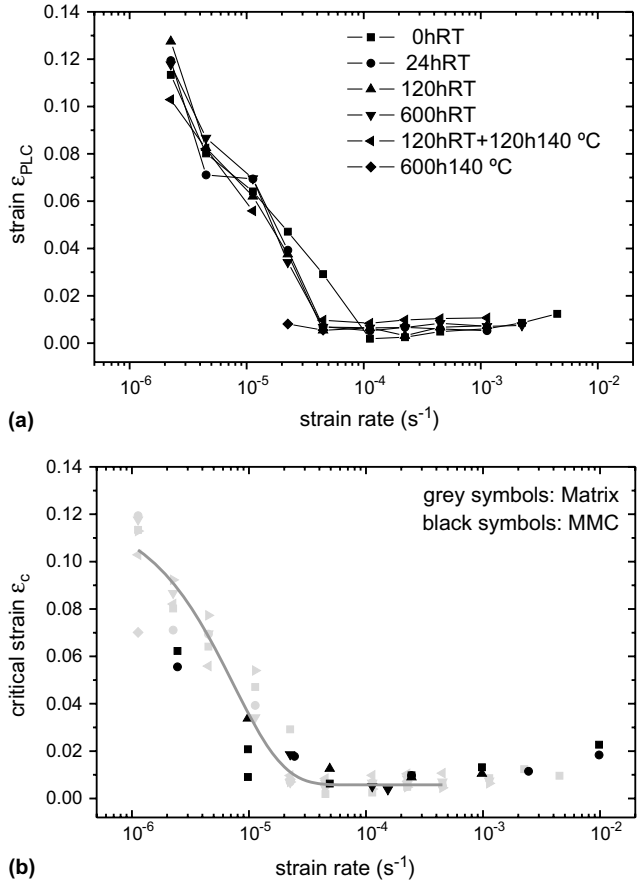

Fig. 4. Critical strain ε_c for the onset of PLC effect vs. applied strain rate for different ageing treatments: (a) matrix material, (b) MMC (the line shows the average matrix behaviour (cf. (a)) for comparison).

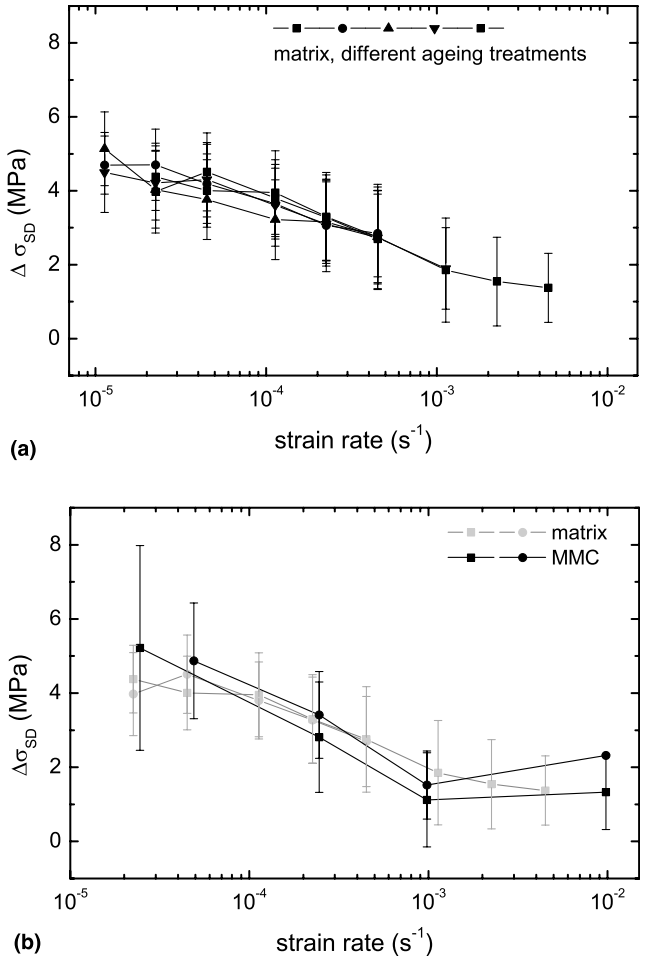

Fig. 5. Depth $\Delta\sigma$ of the stress drops at 5% strain: (a) matrix material (different ageing treatments), (b) MMC (with matrix behaviour for comparison).

increase of the critical strain by particles may be detected in Fig. 4(b) for high strain rates, but it scarcely exceeds the scattering of the values.

3.3. Intensity of serrations

The size of the dislocation avalanches developed during the plastic instability events is roughly reflected in the magnitude of load drops recorded during continuous deformation (neglecting the effects of machine stiffness and of dynamic effects [44]). As shown in Fig. 5 the annealing treatment as well as the alumina obstacles do not result in a significant reduction of the avalanche sizes for the same reasons as discussed in Section 3.2. The general decrease of $\Delta\sigma$ with increasing strain rate is due to the more rapid reloading by the machine drive at higher strain rates after each load drop.

4. Modelling

4.1. Constitutive equations and FE implementation

The macroscopic model presented in [19] is applied to simulate instabilities in materials containing interstitial or substitutional elements that can segregate at dislocations and lock them. It incorporates several features of the intrinsic behaviour of strain ageing materials in a set of phenomenological constitutive equations. The evolution equations try to mimic the mechanisms of repeated breakaway of mobile dislocations temporarily arrested at forest obstacles and of the solute atoms diffusing to (or along) the dislocation cores. Here just a few points should be emphasized, a more detailed description can be found in [45].

At each moment, the flow stress σ is given by

$$\sigma = \sigma_y + Q[1 - \exp(-b\varepsilon_p)] + P_1\, C_s,$$
$$C_s = C_m[1 - \exp(-P_2\varepsilon_p^{\alpha} t_a^{n})] \quad (1)$$

where $\sigma_y + Q[1 - \exp(-b\varepsilon_p)]$ describes yield stress σ_y and isotropic strain hardening by the material parameters σ_y and Q, b characterizes work hardening and ε_p is the equivalent plastic strain variable. The instantaneous strain rate sensitivity is neglected in the yield stress term because it is near zero for PLC conditions [19]. The isotropic strain ageing term $P_1 C_s$ corresponds to the stress associated with DSA. It depends on the local plastic strain rate through the

time t_a (ageing time) that a dislocation spends at localized obstacles when it gets additionally pinned by solutes diffusing to its core. C_s is the concentration of solute atoms segregating around the dislocation lines which are temporarily immobilized by extrinsic obstacles. C_m is the saturated (maximum) concentration around the dislocations. P_1, P_2, α and n are material parameters in Eq. (1) characterizing the influence of DSA. An exponent n equal to 1/3 instead of the Cottrell Bilby exponent 2/3 is adopted in view of the more probable "pipe diffusion" of solute atoms along dislocation lines [11,12,46].

The transition from low to high solute concentration C_s at the dislocations, occurring during the segregation process is approximated by the "relaxation–saturation" kinetics [47] (applied here instead of the differential equation suggested by [14], which would be physically more realistic, but more complex to implement in the calculations, and would yield similar results).

$$\dot{t}_a = \frac{t_w - t_a}{t_w}, \quad t_w = \frac{\Omega}{\dot{\varepsilon}_p} \tag{2}$$

The time t_w is the mean waiting time of dislocations, which are temporarily stopped by extrinsic obstacles. It depends on the plastic strain rate ($t_w \propto 1/\dot{\varepsilon}_p$, if the mobile dislocation density is assumed to be constant). The parameter Ω represents the elementary strain that all mobile dislocations can produce collectively upon depinning. Ω is assumed to be constant in a very first approximation [19], in view of contradicting behaviours discussed in the literature [48,49].

The previous model is implemented in the FE program Zset [50]. The differential equations are integrated at each Gauss point using a fourth order Runge–Kutta method with automatic timestepping. The resolution method for global balance is based on an implicit Newton algorithm.

4.2. Simulation results

In this section we first have to prove, if the model is able to reproduce the PLC behaviour of the bulk Al–Mg alloy, in particular the strain rate dependence of the PLC types. Three strain rates have been selected representing PLC type A (continuous movement of deformation bands, $\dot{\varepsilon} = 1 \times 10^{-3}\,s^{-1}$) and type B (intermittent propagation, $\dot{\varepsilon} = 1 \times 10^{-4}\,s^{-1}$ and $1 \times 10^{-5}\,s^{-1}$, the latter with some stable deformation at the beginning). A 2-dimensional FE analysis is carried out for straight specimens with a total length of 12.5 mm and a width of 2.5 mm. 8-nodes quadratic elements are used with reduced integration under plane stress conditions. As a boundary condition the vertical displacement at the bottom is fixed to zero, the vertical displacement at the top is defined by a constant displacement rate. An initial defect (lower yield stress) is introduced in a single element in the center of the specimen in order to trigger the first plastic strain rate bands. The position and the value of this defect do not change significantly the simulation results [51].

From simulations of uniaxial tensile tests at various applied strain rates (and at room temperature) we can derive by comparison of measured matrix data and calculated behaviour the material parameters like yield stress σ_y and the hardening rate (Q, b). Using these material parameters we have to find the parameters P_1 and P_2 and Ω, which control the PLC behaviour in our simulations. The result is shown in Fig. 6. One can see that in case of

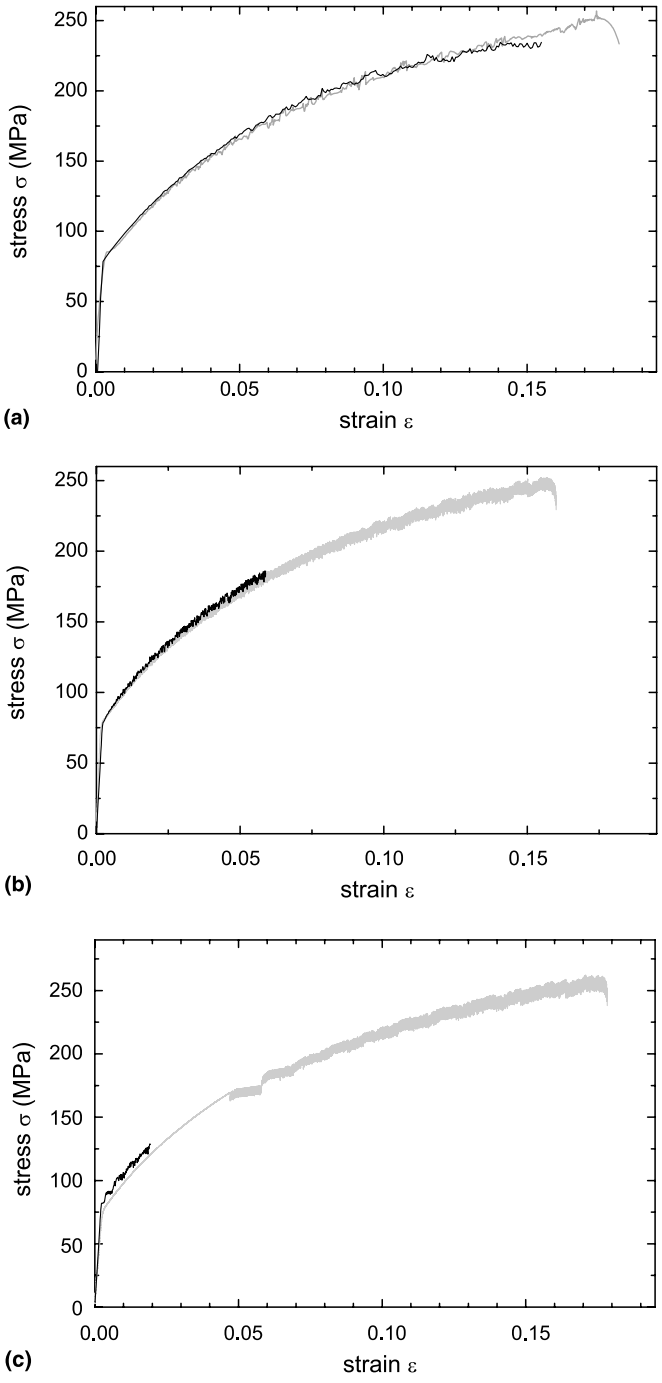

Fig. 6. Comparison between experimental data (matrix, grey) and the simulation results (black) for various applied strain rates: (a) PLC type A ($\dot{\varepsilon} = 1 \times 10^{-3}\,s^{-1}$), (b) PLC type B ($\dot{\varepsilon} = 1 \times 10^{-4}\,s^{-1}$), and (c) type B preceded by smooth deformation up to ε_c($\dot{\varepsilon} = 1 \times 10^{-5}\,s^{-1}$).

PLC type A ($\dot{\varepsilon} = 1 \times 10^{-3}\ s^{-1}$) and type B ($\dot{\varepsilon} = 1 \times 10^{-4}\ s^{-1}$) the simulation fits quite well to the experimental data, whereas the smooth deformation prior to type B serrations at the lowest strain rate ($\dot{\varepsilon} = 1 \times 10^{-5}\ s^{-1}$) could not be simulated adequately. This is expected because the model equations (Section 4.1) are not designed for the description of an "inverse" PLC behaviour.

In order to apply the material parameters to the MMC an appropriate structure of finite elements has to be chosen. For the sake of simplicity at first a 2D unit cell corresponding to a hexagonal distribution of next nearest neighbouring particles is used. The particles are simulated as disks with a very high elastic modulus and are tightly fixed to the matrix. The periodic alignment of particles reflects just the density and not the true arrangement of particles, but provides a good approximation of the behaviour at least for small volume fractions. The influence of the used mesh density and the constraint to periodicity were found to be negligible [51].

In Fig. 7 the computed stress–strain curves of the MMCs for an applied strain rate of $\dot{\varepsilon} = 1 \times 10^{-3}\ s^{-1}$ are compared with the results for the matrix material AA5754. From classical theory the introduction of non-shearable particles into the matrix is expected to increase the macroscopic stress values, because the amount of "soft" material is reduced. In addition, the presence of particles should constrain the movement of dislocation avalanches, so that the amplitude of the serrations should be reduced and the onset of PLC effect should be retarded, i.e. ε_c is expected to increase. However, the critical strain ε_c for the onset is slightly reduced. This behaviour, as well as the observation that the yield stress is nearly unaffected by the volume fraction of particles, can be explained again by stress concentrations in the surrounding of the particles. In the simulations first plastic strain events have been detected at macroscopic stresses 10–15 MPa below the yield stress found for the matrix material.

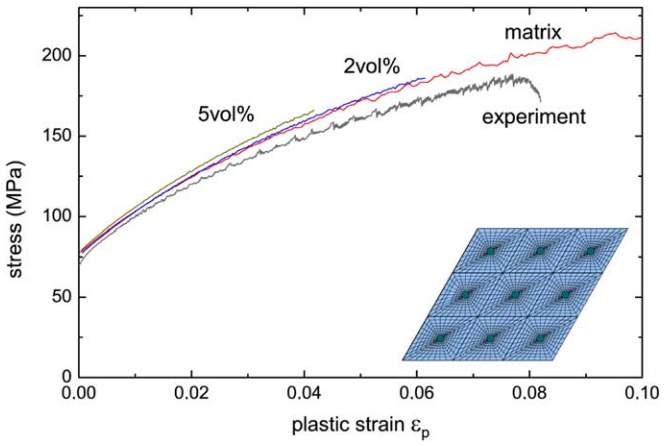

Fig. 7. Influence of the volume fraction of particles at $\dot{\varepsilon} = 1 \times 10^{-3}\ s^{-1}$. The inset indicates the hexagonal arrangement of the unit cells, though for these calculations just one unit cell with periodic boundary conditions has been used.

For comparison, in Fig. 7 also an experimental stress–strain curve for the MMC material is shown. The experimental stress level is below the calculated values, probably caused by micro-cracks inside the clusters of particles [43], which reduce the effective cross-section and thus increase the local stress significantly.

5. Discussion and outlook

In parallel to tensile experiments a strain ageing model implemented in a FE code is used to investigate the influence of Al_2O_3 particles in an Al–3%Mg alloy (AA5754). Parameters for the successful simulation of the observed PLC type A (continuous propagation of PLC bands) and type B (intermittent propagation) are found while the observed "inverse" behaviour for small strain rates (where the PLC serrations start at higher critical strain after smooth deformation) cannot be simulated as it is not contained in the constitutive model equations. According to [18] this would require to describe the kinetics of the additional obstacle enthalpy due to diffusion of solutes to the dislocations waiting for thermal activation, as well as the kinetics of dislocation density evolution including the long-range dislocation interactions, as proposed in [14,15].

Applying the simplified model to the AA5754 MMC and using a periodic arrangement of inclusions it has been found that the introduction of non-shearable particles reduces in the simulations the amplitude of stress drops significantly by obstruction of the movement of dislocation avalanches, but does not prevent these avalanches due to still large areas of pure matrix between the inclusions. In the experiments, the strongly inhomogeneous distribution of inclusions and local stress concentrations cause the persistence of shear instabilities in the MMC material.

The critical strain ε_c for the onset of PLC effect was found to be slightly reduced in the simulations caused by stress concentrations in the surrounding of the particles. ε_c increases again with increasing volume fraction of particles, probably due to an increase of the mean strain rate in the "soft" material caused by the increase of the volume fraction of "hard" material (particle).

The assumed periodic arrangement of inclusions is expected to be unfavourable for suppressing avalanches due to the possibility of far-reaching avalanches running between rows of particles. Indeed, first simulations using a random distribution of particles show a further reduction of the size of the serrations, but still localized deformation bands can be found [51]. This behaviour will be investigated in future analysis.

The experiments described as well as the simulations suggest that for further reduction of the PLC serrations the density of (non-shearable) obstacles should be higher and more homogeneous in distribution. This might be achieved by precipitation of an appropriate phase during thermal treatments.

Since the AA5754 alloy does not show significant improvements by annealing, further experiments are per-

formed using a different Al–Mg alloy (e.g. AA6061) with a stronger and more rapid age hardening ability.

Acknowledgements

The authors wish to thank the DFG and the EU (DEFINO RTN network) for their financial support of our research.

References

[1] J. Caisso, Rev. Metall. LVI (3) (1959) 237.
[2] P.G. McCormick, Acta Metall. 19 (1971) 463.
[3] P.G. McCormick, Acta Metall. 20 (1972) 351.
[4] K. Chihab, Y. Estrin, L.P. Kubin, J. Vergnol, Scripta Met. 21 (1987) 203.
[5] J. Balik, P. Lukac, Acta Metall. Mater. 41 (1993) 1447.
[6] F.B. Klose, F. Hagemann, P. Hähner, H. Neuhäuser, Mater. Sci. Eng. A 387–389 (2004) 93.
[7] L.P. Kubin, C. Fressengeas, G. Ananthakrishna, in: F.R.N. Nabarro, M.S. Duesberry (Eds.), Dislocations in Solids, vol. 11, North Holland Publ. Comp., Amsterdam, 2002, p. 101.
[8] J. Balik, P. Lukac, Czech. J. Phys. B39 (1989) 447, and 1138.
[9] J. Balik, P. Lukac, Kovove Mater. 36 (1998) 162.
[10] P.G. McCormick, C.P. Ling, Acta Metall. Mater. 43 (1995) 1969.
[11] Ch. Schwink, A. Nortmann, Mater. Sci. Eng. A 234–236 (1997) 1.
[12] F. Springer, A. Nortmann, Ch. Schwink, Phys. Stat. Sol. (A) 170 (1998) 63.
[13] P. Hähner, Mater. Sci. Eng. A 207 (1996) 208, and 216.
[14] P. Hähner, Acta Metall. Mater. 45 (1997) 3695.
[15] P. Hähner, A. Ziegenbein, E. Rizzi, H. Neuhäuser, Phys. Rev. B 65 (2002) 134109.
[16] M. Abbadi, P. Hähner, A. Zeghloul, Mater. Sci. Eng. A 337 (2002) 294.
[17] F.B. Klose, A. Ziegenbein, F. Hagemann, H. Neuhäuser, P. Hähner, M. Abbadi, A. Zeghloul, Mater. Sci. Eng. A 369 (2004) 76.
[18] F.B. Klose, PhD thesis, Technische Universität Braunschweig, http://opus.tu-bs.de/opus/volltexte/2004/571/.
[19] S. Zhang, P.G. McCormick, Y. Estrin, Acta Mater. 49 (2000) 1087.
[20] S. Kok, A.J. Beaudoin, D.A. Tortorelle, M. Lebyodkin, Model. Simul. Mater. Sci. Eng. 10 (2002) 1.
[21] S. Kok, M.S. Bharati, A.J. Beaudoin, C. Fressengeas, G. Ananthakrishna, L.P. Kubin, M. Lebyodkin, Acta Mater. 51 (2003) 3651.
[22] E. Rizzi, P. Hähner, Acta Mater. 51 (2003) 3385.
[23] E. Rizzi, P. Hähner, Int. J. Plasticity 20 (2004) 121.
[24] G. Lasko, P. Hähner, S. Schmauder, Model. Simul. Mater. Sci. Eng. 13 (2005) 645.
[25] E. Pink, in: P.O. Kettunen, T.K. Lepistö, M.E. Lehtonen (Eds.), Proc. ICSMA-8, vol. 1, Pergamon, 1988, p. 485.
[26] E. Pink, Acta Metall. 37 (1989) 1773.
[27] E. Pink, J. Krol, Acta Metall. Mater. 43 (1995) 2351.
[28] M. Cieslar, P. Vostry, I. Stulikova, Phys. Stat. Sol. (A) 157 (1996) 257.
[29] F. Chmelik, J. Balik, P. Lukac, E. Pink, M. Cepova, Mater. Sci. Forum 217–222 (1996) 1019.
[30] P. Lukac, J. Balik, F. Chmelik, Mater. Sci. Eng. A 234–236 (1997) 45.
[31] Y. Brechet, Y. Estrin, Acta Metall. Mater. 43 (1995) 955.
[32] A. Luft, Prog. Mater. Sci. 35 (1991) 91.
[33] H. Neuhäuser, in: F.R.N. Nabarro (Ed.), Dislocations in Solids, vol. 6, North-Holland P.C., Amsterdam, 1983, p. 379.
[34] D. Thevenet, M. Mliha-Touati, A. Zeghloul, Mater. Sci. Eng. A 266 (1999) 175.
[35] D. Thevenet, M. Mliha-Touati, A. Zeghloul, Mater. Sci. Eng. A 291 (2000) 110.
[36] R. Shabadi, S. Kumar, H.J. Roven, E.S. Dwarakadasa, Mater. Sci. Eng. A 364 (2004) 140.
[37] R. Shabadi, S. Kumar, H.J. Roven, E.S. Dwarakadasa, Mater. Sci. Eng. A 382 (2004) 203.
[38] Q. Zhang, Z. Jiang, H. Jiang, Z. Chen, X. Wu, Int. J. Plasticity 21 (2005) 2150.
[39] W. Tong, H. Tao, N. Zhang, L.G. Hector, Scripta Mater. 53 (2005) 87.
[40] H. Ait-Amokhtar, S. Boudrahem, C. Fressengeas, Scripta Mater. 54 (2006) 2193.
[41] J. Balik, P. Lukac, L.P. Kubin, Scripta Mater. 42 (2000) 465.
[42] Y. Estrin, M.A. Lebyodkin, Mater. Sci. Eng. A 387–389 (2004) 195.
[43] E. Soppa, S. Schmauder, G. Fischer, J. Brollo, U. Weber, Comp. Mater. Sci. 28 (2002) 574.
[44] R.B. Schwarz, L.L. Funk, Acta Metall. 33 (1985) 295.
[45] S. Graff, S. Forest, J.-L. Strudel, C. Prioul, P. Pilvin, J.-L. Béchade, Mater. Sci. Eng. A 387–389 (2004) 191.
[46] J. Friedel, Dislocations, Pergamon Press, 1964, p. 351.
[47] P.G. McCormick, Y. Estrin, Acta Metall. Mater. 39 (1991) 2977.
[48] L.P. Kubin, Y. Estrin, Acta Metall. Mater. 38 (1990) 697.
[49] F. Springer, Ch. Schwink, Scripta Metall. Mater. 25 (1991) 2739.
[50] www.nwnumerics.com, www.mat.ensmp.fr, Z-set package, 1996.
[51] S. Graff, H. Dierke, S. Forest, H. Neuhäuser, J.-L. Strudel, C. Prioul, J.-L. Béchade (in preparation).